International Journal of Greenhouse Gas Control 3 (2009) 368–375

Contents lists available at ScienceDirect

International Journal of Greenhouse Gas Control

journal homepage: www.elsevier.com/locate/ijggc

# Numerical simulation of chemical looping combustion process with $CaSO_4$ oxygen carrier

Zhongyi Deng *, Rui Xiao, Baosheng Jin, Qilei Song

*Key Laboratory of Clean Coal Power Generation and Combustion Technology of Ministry of Education, Southeast University, Nanjing 210096, China*

ARTICLE INFO

*Article history:*
Received 19 May 2008
Received in revised form 17 November 2008
Accepted 21 November 2008
Available online 4 January 2009

*Keywords:*
Chemical looping combustion
CFD modeling
$CO_2$ capture
$CaSO_4$

ABSTRACT

Chemical-looping combustion (CLC) is a promising technology for the combustion of gas or solid fuel with efficient use of energy and inherent separation of $CO_2$. The technique involves the use of an oxygen carrier which transfers oxygen from combustion air to the fuel, and hence a direct contact between air and fuel is avoided. A chemical-looping combustion system consists of a fuel reactor and an air reactor. A metal oxide is used as oxygen carrier that circulates between the two reactors. The air reactor is a high velocity fluidized bed where the oxygen carrier particles are transported together with the air stream to the top of the air reactor, where they are then transferred to the fuel reactor using a cyclone. The fuel reactor is a bubbling fluidized bed reactor where oxygen carrier particles react with hydrocarbon fuel and get reduced. The reduced oxygen carrier particles are transported back to the air reactor where they react with oxygen in the air and are oxidized back to metal oxide. The exhaust from the fuel reactor mainly consists of $CO_2$ and water vapor. After condensation of the water in the exit gas from the fuel reactor, the remaining $CO_2$ gas is compressed and cooled to yield liquid $CO_2$, which can be disposed of in various ways.

With the improvement of numerical methods and more advanced hardware technology, the time needed to run CFD (Computational fluid dynamics) codes is decreasing. Hence multiphase CFD-based models for dealing with complex gas-solid hydrodynamics and chemical reactions are becoming more accessible. Until now there were a few literatures about mathematical modeling of chemical-looping combustion using CFD approach. In this work, the reaction kinetics model of the fuel reactor ($CaSO_4 + H_2$) was developed by means of the commercial code FLUENT. The bubble formation and the relation between bubble formation and molar fraction of products in gas phase were well captured by CFD simulation. Computational results from the simulation also showed low fuel conversion rate. The conversion of $H_2$ was about 34% partially due to fast, large bubbles rising through the reactor, low bed temperature and large particles diameter.



## 1. Introduction

Carbon dioxide emissions derived from human activities have increased the concentration of greenhouse gases in the atmosphere, contributing to global climate change. While the effects on global climate are uncertain, many scientists agree that there could be serious environmental consequences. About a third of the global $CO_2$ emissions come from the burning of fossil fuels in power production. There is an urgent need for developing new clean energy technologies to control the greenhouse gas with less energy loss.

As we known, fuel and air are directly mixed and burned in the conventional system which gives rise to emission of carbon dioxide, nitrogen oxides, and so on. There is a worldwide interest in capturing and sequestering the carbon dioxide ($CO_2$) generated in those conventional fossil fuel combustion processes due to increasing concern over the concentration of $CO_2$ in the atmosphere. However, most of these technologies require a large amount of energy to separate and collect $CO_2$ from the exhaust gas because $CO_2$ is diluted by $N_2$ in air in the conventional system. Chemical-looping combustion (CLC) has been proposed as a new technology which provides a sequestration ready $CO_2$ stream with no additional energy required for separation (Richter and Knoche, 1983). Many research works including the oxygen carrier development, system analysis and the reactor design have been carried out on this field (Johansson et al., 2006a). Chemical looping combustion (CLC) process would be a good candidate for the production of clean energy from fossil fuel.

The major advantage of the CLC system which is to provide a sequestration ready $CO_2$ stream with no additional energy required for separation For option of the $CO_2$ recovery and sequestration, so far, there have been many technologies such as

* *Corresponding author.*
*E-mail address:* dzyseu@gmail.com (Z. Deng).

1750-5836/$ – see front matter. 
doi:10.1016/j.ijggc.2008.11.004

**Nomenclature**

| | |
|---|---|
| $d_p$ | diameter(m) |
| $D_{m,i}$ | diffusion coefficient of the mixture ($m^2/s$) |
| $e$ | coefficient of restitution |
| $E$ | activation energy (kJ/kmol) |
| $g_0$ | radial distribution function |
| $h_{sg}$ | heat transfer coefficient($W/m^2$ K) |
| $H_i$ | enthalpy (J/kg) |
| $J_{g,i}$ | diffusion flux ($kg/m^2$ s) |
| $Q_{sg}$ | intensity of heat exchange between the gas and solid phases ($W/m^2$) |
| $K_i$ | apparent kinetic constant |
| $N_u$ | Nusselt number |
| $Sc$ | Schmidt number |
| $Pr$ | Prandtl number |
| Re | Reynolds number |
| $r_c$ | the reaction rate |
| $S$ | source term |
| $T$ | temperature (K) |
| $U_{mf}$ | minimum fluidization velocity (m/s) |
| $V$ | the instantaneous velocity (m/s) |
| $P$ | pressure (Pa) |
| $X_i$ | molar fraction |
| $u$ | the mean velocity (m/s) |
| $Y_i$ | the mass fraction |
| $Z_i$ | conversion |

*Greek symbols*

| | |
|---|---|
| $\varepsilon$ | volume fraction |
| $\rho$ | density ($kg/m^3$) |
| $\lambda$ | thermal conductivity of mixture (W/m K) |
| $\tau_g$ | stress tensor (Pa) |
| $\gamma$ | dissipation of fluctuating energy ($W/m^3$) |
| $\beta$ | the drag coefficient ($kg/m^3$ s) |
| $\mu$ | viscosity (kg/m s) |
| $\xi_s$ | solid bulk viscosity (Pa s) |

*Subscripts*

| | |
|---|---|
| s | solid phase |
| g | gas phase |
| $i$ | the $i$th species |
| $i$, $j$, $k$ | direction coordinates |

absorption (MEA, Selexol), adsorption (PSA, TSA), membranes, or cryogenics etc. Most of these technologies, however, require a large amount of energy.

Recent studies in this novel technology (Ryu et al., 2001; Ishida et al., 2002; Adánez et al., 2003, 2004; Mattisson et al., 2004; Cho et al., 2004; Abad et al., 2006; Johansson et al., 2006b) have been focused in three distinct areas: techno-economic evaluations, integration of the system into power plant concepts, and experimental development of oxygen carrier metals such as Fe, Ni, Mn, Cu, and Ca. The oxygen carrier is a core technology in the CLC system. The current oxygen carriers are metal oxides which have high reactivity and stability. However, these metal-oxide oxygen carriers will inevitably have some leakage to the environment and become second pollution sources.

As a novel oxygen carrier, $CaSO_4$ oxygen carrier has many advantages that enable it interesting for use in the CLC system. It seems more environmentally benign than most of the proposed metal oxidized systems, and there are large amounts of natural gypsum available worldwide. $CaSO_4$ has a relative higher oxygen capacity compared to metal oxides. The oxygen ratio shows the maximum amount of oxygen that can be transferred between the air and fuel reactors. The theoretical oxygen ratio for $CaSO_4$/CaS is 0.4706, which is much higher than that of metal oxides (Mattisson et al., 2003). As one of gypsum resources, natural anhydrite ore is consisted of high purity of $CaSO_4$ and has a relative higher mechanical strength compared to synthesized calcium based oxygen carrier particles in our previous studies and may be suitable for application in fluidized bed reactor of CLC systems.

As shown in the Figs. 1 and 2, a chemical-looping combustion system consists of a fuel reactor and an air reactor. The air reactor is a high velocity fluidized bed where the oxygen carrier particles are transported together with the air stream to the top of the air reactor, where they are then transferred to the fuel reactor using a cyclone. The fuel reactor is a bubbling fluidized bed reactor, from which the reduced oxygen carriers are transported back to the air reactor by means of an overflow pipe. After condensation of the water in the exit gas from the fuel reactor, the remaining $CO_2$ gas is compressed and cooled to yield liquid $CO_2$, which can be disposed of in various ways.

It consists of two continuous reactions as shown in the following formulae (1) and (2). The reduction product CaS of a oxygen carrier ($CaSO_4$) obtained according to the formula (1) is utilized in the oxidation reaction of the formula (2). Therefore, it is a chemical-looping reaction with $CaSO_4$ as an oxygen carrier. The reaction of the formula (1) is an exothermic reaction of $CaSO_4$ and a fuel ($H_2$) with low-level energy release in a low-temperature region (about 600–1200 K) and the reaction of the second step is an exothermic oxidation of the reaction product (CaS) of the first step in a high-temperature region (about 800–1700 K). A high-temperature exhaust gas is produced by the heat of the reaction.

Calcium sulfate ($CaSO_4$) is reduced by hydrogen ($H_2$) to calcium sulfide (CaS) in the fuel reactor (bubbling fluidized bed):

$$CaSO_4 + 4H_2 \rightarrow CaS + 4H_2O \quad (1)$$

Then CaS is transported to the air reactor (circulating fluidized bed) to be oxidized back to $CaSO_4$:

$$CaS + 2O_2 \rightarrow CaSO_4 \quad (2)$$

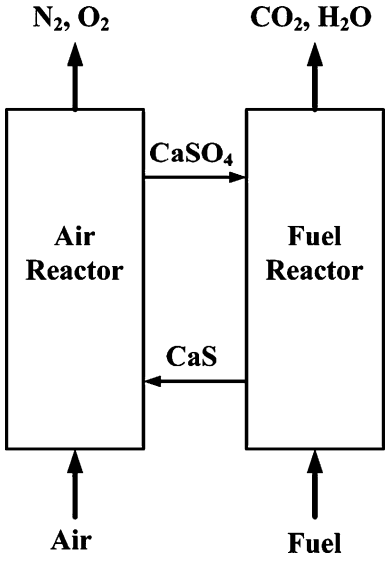


**Fig. 1.** Concept view of chemical-looping combustion using $CaSO_4$ as oxygen carrier.

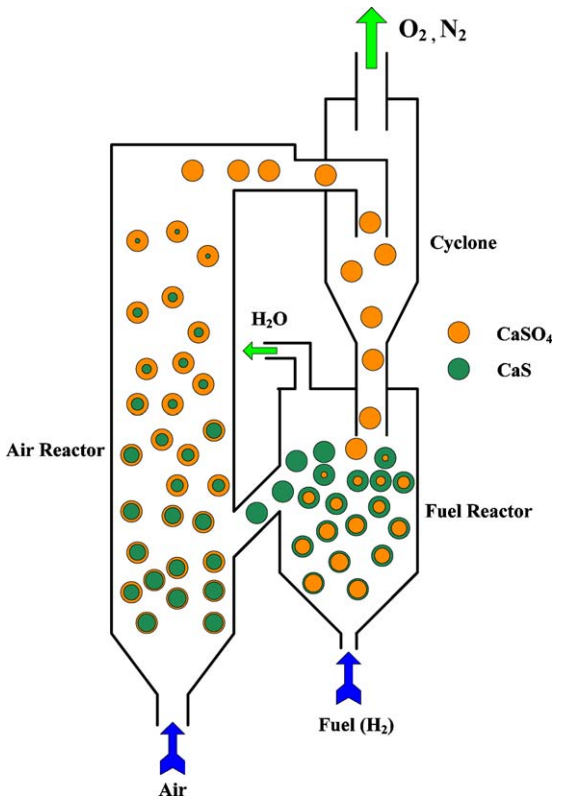


**Fig. 2.** Chemical-looping combustion with two interconnected fluidized bed reactors.

The flue gas from the air reactor contains nitrogen and any unreacted oxygen.

With the improvement of numerical methods and more advanced hardware technology, the time needed to run CFD codes is decreasing. Hence the multi-dimensional models for dealing with complex gas-solid hydrodynamics, heat transfer and chemical reactions are becoming more accessible. Once the model has been validated, CFD can be used to make sensitivity analysis as it provides the flexibility to change parameters. A series of unsteady, three-fluid CFD model were performed using FLUENT 6.0 by Scott et al. (2005) to simulate particle mixing in a binary fluidized bed. Ravelli et al. (2008) proposed a mathematical model to simulate the combustion of refuse-derived fuel (RDF) in bubbling fluidized bed by means of the commercial code FLUENT 6.1 and the comparison between the predicted and the experimental data were in agreement. Frazeli and Behnam (2007) proposed a CFD model to predict methane autothermal in a catalytic microreactor.

Our recent thorough literature review shows that multiphase fluid dynamics modeling for CLC is not available in the open literature by FLUENT. In this study, the reaction kinetics model of the fuel reactor ($CaSO_4$+ $H_2$) has been developed to mimic the behavior of reactive flow in the reactors.

This computational approach is a significant first step in the systematic analysis of CLC to assess its potentiality to be integrated in the next generation of fossil fuel power plants.

## 2. Mathematical model

The main assumptions of this model are:

(1) It includes two phases: gas and solid.
(2) The particles in the bed are spherical and uniform in size
(3) The particles are assumed inelastic, smooth and monodispersed spheres.
(4) The kinetic theory of granular flow (KTGF) is used in transport equation to describe the particles collision and fluctuation in the bed.
(5) In this work, the reaction temperature is 850 °C. The side reactions are greatly suppressed. So we ignored the side reactions.

### 2.1. Gas–solid hydrodynamics

#### 2.1.1. Continuity equations

$$\frac{\partial}{\partial t}\left(\varepsilon_g \rho_g\right) + \nabla \cdot \left(\varepsilon_g \rho_g V_g\right) = S_{gs}$$

$$\frac{\partial}{\partial t}(\varepsilon_s \rho_s) + \nabla \cdot (\varepsilon_s \rho_s V_s) = S_{sg}$$

where $\varepsilon$, $\rho$ and $V$ are the volume fraction, the density and the instantaneous velocity, respectively. The instantaneous velocity of particles $V_s$ can be substituted by the solid mean velocity $u_s$. This form was also derived from the Boltzmann integral–differential equation by Ding and Gidaspow (1990). $S$ is the source term and set to zero only in flow field. When the continuity equations are used in heterogeneous reaction, there is the mass, momentum and heat exchange between gas phase and solid phase.

#### 2.1.2. Momentum equations

For the gas phase:

$$\frac{\partial}{\partial t}\left(\varepsilon_g \rho_g V_g\right) + \nabla \cdot \left(\varepsilon_g \rho_g V_g V_g\right) = -\varepsilon_g \nabla P + \varepsilon_g \rho_g g + \nabla \cdot \varepsilon_g \tau_g - \beta_{gs}(V_g - u_s) + S_{gs} u_s$$

where $\beta_{gs}$ is the drag coefficient between the gas phase and solid phase, $g$ is gravity and $u_s$ is the mean velocity. In the right hand of the equations, the fifth term $S_{gs}u_s$ describes the momentum transfer of the solid.

The momentum equation for the solid phase should obtain the reverse source term and can be expressed as:

$$\frac{\partial}{\partial t}(\varepsilon_s \rho_s V_s) + \nabla \cdot (\varepsilon_s \rho_s V_s V_s) = -\varepsilon_s \nabla P + \varepsilon_s \rho_s g - \nabla P_s + \nabla \cdot \varepsilon_s \tau_s + \beta_{gs}(V_g - u_s) + S_{sg} u_s$$

#### 2.1.3. Energy equations

$$\frac{\partial}{\partial t}(\varepsilon_g \rho_g H_g) + \nabla \cdot (\varepsilon_g \rho_g u_g H_g) = \nabla(\lambda_g \nabla T_g) + Q_{gs} + S_{gs} H_s$$

$$\frac{\partial}{\partial t}(\varepsilon_s \rho_s H_s) + \nabla \cdot (\varepsilon_s \rho_s u_s H_s) = \nabla(\lambda_s \nabla T_s) + Q_{sg} + S_{sg} H_s$$

where $H$, $\lambda$ and $Q$ are enthalpy, thermal conductivity of mixture and heat exchange between gas phase and solid phase, respectively. The third term on the right hand is the heat transfer in that the solid phase changed into gas phase.

The heat exchange between phases can be expressed as a function of the temperature difference and conform to the local balance condition $Q_{sg} = -Q_{gs}$

$$Q_{sg} = h_{sg}(T_s - T_g)$$

$h_{sg}$ is heat transfer coefficient, which is relative to the $Nu_s$ of solid phase.

$$h_{sg} = \frac{6 k_g \varepsilon_s \varepsilon_g Nu_s}{d_p^2}$$

$k_g$ is thermal conductivity of gas and $Nu_s$ was proposed by Gunn (1978).

$$Nu_s = (7 - 10\varepsilon_g + 5\varepsilon_g^2)(1 + 0.7Re_s^{0.2}Pr^{1/3}) + (1.33 - 2.4\varepsilon_g + 1.2\varepsilon_g^2)Re_s^{0.7}Pr^{1/3}$$

#### 2.1.4. Kinetic theory of granular flow (KTGF)

A transport equation which describes particles collision resulting in a random granular motion is defined for solid phase (Patil et al., 2005):

$$\frac{\partial}{\partial t}(\varepsilon_s\rho_s\Theta_s) + \nabla\cdot(\varepsilon_s\rho_s\Theta_s\vec{u}_s) = -\frac{2}{3}(p_s\bar{\bar{I}} + \varepsilon_s\overline{\overline{\tau_s}}) : \nabla\vec{u}_s + \nabla\cdot(k_s\nabla\Theta_s) - \gamma - 3\beta_{gs}\Theta_s$$

Here, $\Theta_s$ is granular temperature and $P_s$ is solid pressure,

$$\Theta = \frac{1}{3}\langle u_s' u_s'\rangle$$

where $u_s'$ is the fluctuating velocity of the particles and can be derived from $u_s' = V_s - u_s$

$$p_s = \varepsilon_s\rho_s\Theta_s + 2(1+e)\varepsilon_s^2 g_0\rho_s\Theta_s$$

The diffusion coefficient for granular energy $k_s$ is given by:

$$k_s = \frac{150\rho_s d_s\sqrt{\Theta_s\pi}}{384(1+e)g_0}\left[1 + \frac{6}{5}\varepsilon_s g_0(1+e)\right]^2 + 2\rho_s\gamma_s^2 d_s g_0(1+e)\sqrt{\frac{\Theta_s}{\pi}}$$

Here $g_0$ is the radial distribution function.

$$g_0 = \frac{3}{5}\left[1 - \left(\frac{\varepsilon_s}{\varepsilon_{s,\max}}\right)^{1/3}\right]^{-1}$$

The dissipation of fluctuating energy due to inelastic collision takes the form:

$$\gamma = 3(1-e^2)\varepsilon_s^2\rho_s d_s g_0\Theta_s\left[\frac{4}{d_s}\left(\sqrt{\frac{\Theta_s}{\pi}}\right) - \nabla u_s\right]$$

The remaining term which needs to be considered is the interphase momentum transfer. It is thought for the drag between gas phase and solid phase to play important role in the momentum exchange. If $\varepsilon_g < 0.8$, the well-known Ergun equation (Gunn, 1978) is suitable for describing the dense regime:

$$\beta_{gs} = 150\frac{(1-\varepsilon_g)r_s\mu_g}{\varepsilon_g d_s^2} + 1.75\frac{\rho_g\varepsilon_s|u_g - u_s|}{d_s}$$

If $\varepsilon_g > 0.8$, the drag coefficient was given based on the work by Wen and Yu (1966)

$$\beta_{gs} = \frac{3}{4}C_d\frac{|u_g - u_s|}{d_s}\varepsilon_g^{-2.65}$$

where

$$C_d = \begin{cases}\dfrac{24}{Re}(1 + 0.15Re^{0.687}), & Re \le 1000\\ 0.44, & Re > 1000\end{cases}$$

$$Re = \frac{|u_g - u_s|\varepsilon_g\rho_g d_s}{\mu_g}.$$

#### 2.1.5. Species transport equations

$$\frac{\partial}{\partial t}\left(\rho_g\varepsilon_g Y_{g,i}\right) + \nabla\left(\rho_g\varepsilon_g V_g Y_{g,i}\right) = -\nabla\cdot\varepsilon_g J_{g,i} + r_i + \varepsilon_g R_{g,i}$$

where $J_{g,i}$, $R_{g,i}$ and $R_{s,I}$ are the diffusion flux of species $i$ in gas phase, the net rate of production of homogeneous species $i$ and the heterogeneous reaction rate, respectively. In the species transport equations of gas phase, mass diffusion coefficients are used to calculate the diffusion flux of chemical species in turbulent flow using modified Fick's law:

$$J_{g,i} = -\left(\rho D_{i,m} + \frac{\mu_t}{Sc_t}\right)\nabla Y_{g,i}$$

where $D_{i,m}$ is diffusion coefficient of the mixture ($m^2/s$).

### 2.2. Constitutive closure models

Constitutive relations are needed to close governing relations. The following are the constitutive relations used in the current model.

The stress tensor of gas phase:

$$\tau_{g,ij} = \mu_g\left(\frac{\partial V_{g,j}}{\partial x,I} + \frac{\partial V_{g,I}}{\partial x,j}\right)$$

The stress tensor of particulate phase:

$$\tau_{s,ij} = \mu_s\left(\frac{\partial V_{s,j}}{\partial x,I} + \frac{\partial V_{s,I}}{\partial x,j}\right) + \left(\xi_s - \frac{2}{3}\mu_p\right)\frac{\partial V_{s,k}}{\partial x,k}\delta_{Ij} - p_s\delta_{Ij}$$

Diffusion coefficient of granular temperature (Syamlal–O'Brien)

$$k_{\Theta s} = \frac{15\cdot d_s\cdot\rho_s\cdot\varepsilon_s\cdot\sqrt{\Theta_s\cdot\pi}}{4\cdot(41-33\eta)} \times\left[1 + \frac{12}{5}\eta^2\cdot(4\cdot\eta - 3)\cdot\varepsilon_s\cdot g_0 + \frac{16}{15\cdot\pi}(41-33\eta)\cdot\eta\cdot\varepsilon_s\cdot g_0\right]$$

$$\eta = \frac{1}{2}(1 + e_{ss})$$

Transfer of kinetic energy:

$$\phi_{gs} = -3\cdot K_{gs}\cdot\Theta_s$$

Solids pressure:

$$p_s = \varepsilon_s\cdot\rho_s\cdot\Theta_s + 2\cdot\rho_s\cdot(1+e_{ss})\cdot\varepsilon_s^2\cdot g_0\cdot\Theta_s$$

Solid shear viscosity:

$$\mu_s = \mu_{s,col} + \mu_{s,kin} + \mu_{s,fr}$$

Solid collision viscosity:

$$\mu_{s,col} = \frac{4}{5}\cdot\varepsilon_s\cdot\rho_s\cdot d_s\cdot g0\cdot(1+e_{ss})\cdot\left(\frac{\Theta_s}{\pi}\right)^{1/2}$$

Solid frictional viscosity:

$$\mu_{s,fr} = \frac{p_s\cdot\sin\phi}{2\cdot\sqrt{I_{2D}}}$$

Kinetic viscosity (Syamlal–O'Brien)

$$\mu_{s,kin} = \frac{d_s\cdot\rho_s\cdot\varepsilon_s\cdot\sqrt{\Theta_s\cdot\pi}}{6\cdot(3-e_{ss})}\left[1 + \frac{2}{5}\cdot(1+e_{ss})\cdot(3\cdot e_{ss} - 1)\cdot\varepsilon_s\cdot g0\right].$$

### 2.3. Fuel reactors kinetic model

A review of the literature by Byung-Su and Hong Yong (2002) presented that the activation energy of the reduction of calcium sulfate to produce calcium sulfide were 151 kJ/mol. The reaction is of first order with respect to hydrogen partial pressure for calcium sulfate.

Initially, the shrinking-core model for grain geometry was applied, which considers the oxygen carriers composed by a matrix of non-porous individual grains of uniform size. This model has been successfully used to describe the reactivity of the particle

previously (Zafar et al., 2007). The kinetic equation for this model relating the conversion and time are:

$$Z_i = \frac{t}{\tau_i}$$

and

$$\frac{dZ_i}{dt} = \frac{1}{\tau_i}$$

where $\tau_i$ is the time for complete conversion of the particle for the reaction $i$ and calculated from

$$\tau_i = \frac{1}{K_i P_{H_2}}$$

where $K_i$ is the apparent kinetic constant (Byung-Su and Hong Yong, 2002).

$$K_c = 4.3 \times 10^3 \, e^{-(151000/RT)}$$

It has been assumed that the reaction rate is first order with respect to hydrogen and is given as follows:

$$r_c = \rho_{m,CaSO_4} \frac{dZ_i}{dt}.$$

## 3. Simulation method

### 3.1. Simulation code and numerical algorithm

Differential equations mentioned in the previous section were solved by a finite volume method. These equations were discretized by an upwind differencing scheme over the used finite volume, and solved by the commercial CFD software code Fluent 6.2.16. A time step of 0.0001 s was chosen. This iteration was adequate to achieve convergence for the majority of time steps. First-order discretization schemes for the convection terms were used. The relative error between two successive iterations was specified by using a convergence criterion of $10^{-3}$ for each scaled residual component. The phase-coupled SIMPLE (PC-SIMPLE) algorithm (Vasquez and Ivanov, 2000), which was an extension of the SIMPLE algorithm to multiphase flows, was applied for the pressure–velocity coupling.

In this algorithm, the coupling terms were treated implicitly and form part of the solution matrix. The pressure–velocity coupling was based on total volume continuity and the effects of the interfacial coupling terms were fully incorporated into the pressure correction equation. Gauss–Seidel method was applied to solve these equations which can be stable due to point by point iteration. In order to reduce the number of iteration and to accelerate the convergence of solution, algebraic multigrid (AMG) scheme was also used to coarsen grids (Tao, 2000).

### 3.2. Boundary and initial conditions

The particles and fuel gas used in the simulation were calcium sulfate and hydrogen, respectively. Table 1 lists main conditions that were applied to simulation.

$k$–$\varepsilon$ turbulence models were selected. The drag coefficient between the gas phase and solid phase that we $k$–$\varepsilon$ used were proposed by Gidaspow et al. (1992). The restitution coefficient between the solid particles was 0.9. The heat transfer coefficient between the gas phase and solid phase we used was proposed by Gunn (1978). For the boundary conditions, we selected velocity-inlet condition for the inlet of reactor and outflow condition for the outlet of reactor. At the walls, a zero gradient condition was used for the turbulent kinetic energy. The no-slip wall condition was used for the gas phase and solid phase (Ding and Gidaspow, 1990). The simulations were carried out with the finite volume method (FVM), in which the inter-phase slip algorithm (IPSA) of Spalding and Markatos (1983) was used to solve velocity–pressure coupled differential equations. For the evaluation of the convective terms, the second order QUICK scheme was used. The time step was set as 0.0001 s.

**Table 1**
Simulation model parameters.

| Description | Value | Comment |
|---|---|---|
| Particle density (kg/m$^3$) | 2960 | Calcium sulfate |
| Gas density (kg/m$^3$) | 0.08189 | Hydrogen |
| Mean particle diameter (mm) | 0.275 | Uniform distribution |
| Initial solids packing | 0.48 | Fixed value |
| Superficial gas velocity (m/s) | 0.32 | $5U_{mf}$ |
| Bed width (m) | 0.25 | Fixed value |
| Bed height (m) | 1 | Fixed value |
| Static bed height (m) | 0.4 | Fixed value |
| Temperature (K) | 1123 | Fixed value |
| Inlet boundary conditions | Velocity | Superficial gas velocity |
| Outlet boundary conditions | Outflow | Fully developed flow |
| Time steps | 0.0001 s | Specified |
| Convergence criteria | $10^{-3}$ | Specified |

As shown in the Fig. 3, the bed was initially filled with particles a 0.4 m high, where the total volume fraction of solids was patched as 0.48 (Chejne and Hernandez, 2002). To prevent the spacing between particles from decreasing to zero, the maximum particle packing was $\varepsilon_{s,max} = 0.6$ (Enwald and Almstedt, 1999). And the 2D computational domain was discretized by 2500 rectangular cells.

## 4. Computational results and discussions

A feed fuel gas consisting of 100 wt.% $H_2$ is fed into the reactor through a distributor. The upward flowing gas bubbles provide the energy to keep the oxygen carrier and fuel gas highly mixed. The reactant ($H_2$) from the gas phase reacts with oxygen ($O_2$) of oxygen carrier and is converted to gas product $H_2O$. The bubble formation is well captured by CFD simulation as shown in Fig. 4. From the simulated frame in Fig. 4, where blue represents pure gas and red mimics dense gas–solid mixture, it could be found most of salient bubble features such as formation, rise and burst. These features influence the amount of fuel burned. For example, the fast bubbles lead to lower reactant conversion rate. The computed flow patterns

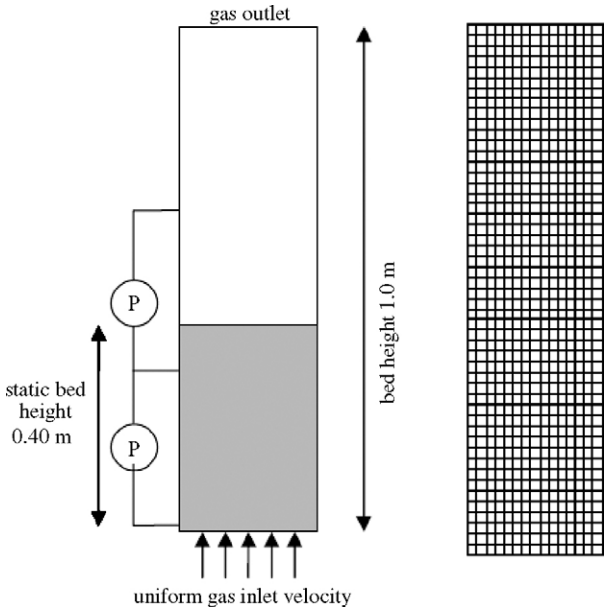


**Fig. 3.** Schematic and grids of the fuel reactor.

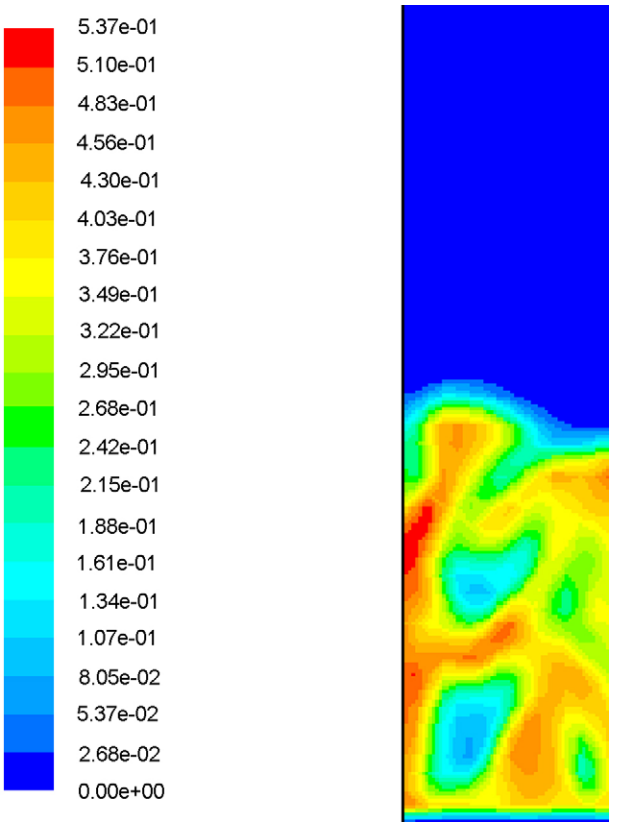


**Fig. 4.** Solid volume fraction.

due to the bubble predicted a global mixing between the gas phase and solid phase in the fuel reactor.

Fig. 5 shows the distributions of reactant and product in terms of molar fraction in gas phase in the quasi-steady state condition at 10 s. It could be found that the profile of reactant ($H_2$) decreases linearly from about 1 around the distributor to 0.6 as the function

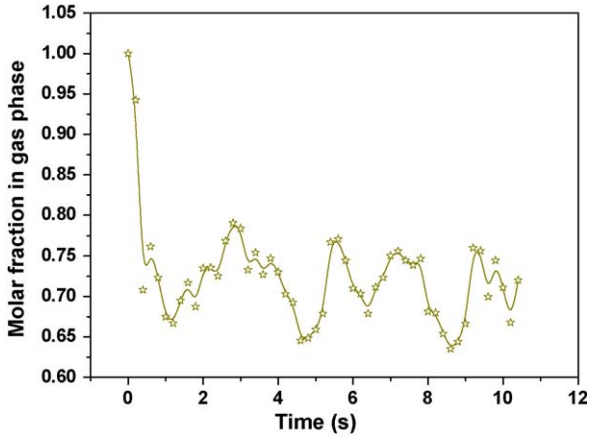


**Fig. 6.** Molar fraction of $H_2$ at 0 cm ($x$) and 30 cm ($y$) of dense bed region.

of bed height until the interface (about 50 cm) between the fluidized regimes and the free board regions. Then it suddenly increases to a constant value of 0.67 in the free board region where the computed solid volume fraction is zero. The reverse is realized for product ($H_2O$).

Fig. 5 also shows a relation between bubble formation and the molar fraction of products in gas phase. It could be found that higher products produced by the reduction-reaction are at the emersion phase where the solid volume fraction is high. The higher reactant of $H_2$ is at the bubble phase. The reaction in the fuel reactor significantly depends on the concentration of the oxygen carrier.

Typical oscillations of fuel reactant ($H_2$) and products ($H_2O$) are computed after the initial 0 s. Fig. 6 shows the time oscillations of fuel gas reactant in the dense bed region. The intense oscillations are due to bubble passage and reaction in the dense region. The hydrogen molar fraction sustains an oscillation around 0.7. Fig. 7 shows similar oscillations of the gas product namely the water vapor. As expected, the product concentration rapidly increases

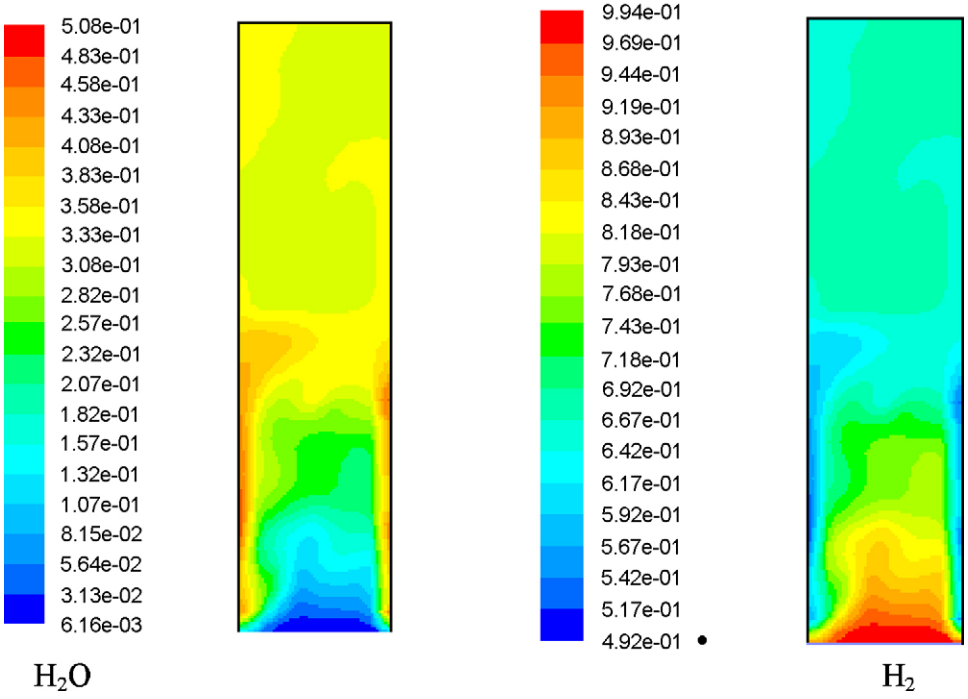


**Fig. 5.** The molar fraction of $H_2O$ and $H_2$.

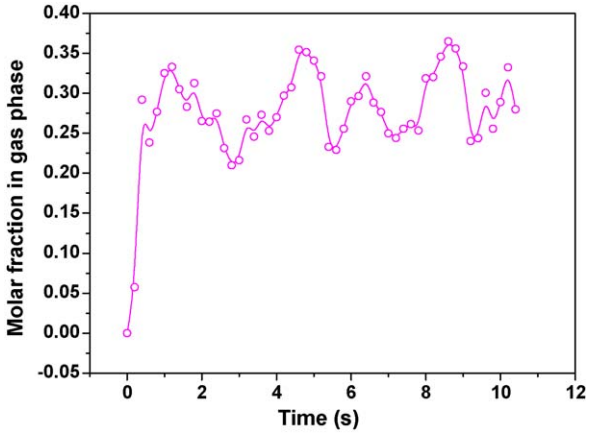


**Fig. 7.** Molar fraction of $H_2O$ at 0 cm ($x$) and 30 cm ($y$) of dense bed region.

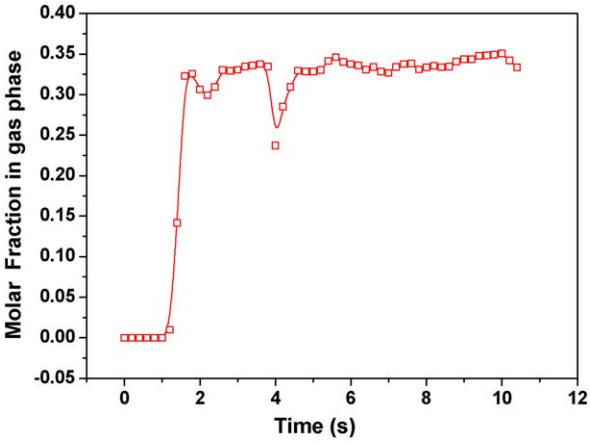


**Fig. 8.** The $H_2O$ molar fraction at outlet.

when the reactant is injected after 0.3 s. However, at about 1.2 s, the product no longer increases and the water vapor molar fraction oscillates around 0.33. This trend indicates that the reaction reached quasi-equilibrium after 1.2 s.

Figs. 8 and 9 exhibit the reactant and product molar fractions at outlet. The gas molar fractions initially oscillate up to 4 s then become nearly constant at around 0.66 for $H_2$ and 0.34 for $H_2O$. The changes of molar fraction of the gas compositions are not as obvious as the dense bed region. This is due to the absence of solid reactant $CaSO_4$ in the free board region. Under this simulation conditions, the conversion of $H_2$ is about 34%. An increased the bed temperature and a decreased the particle size would increase the conversion rate.

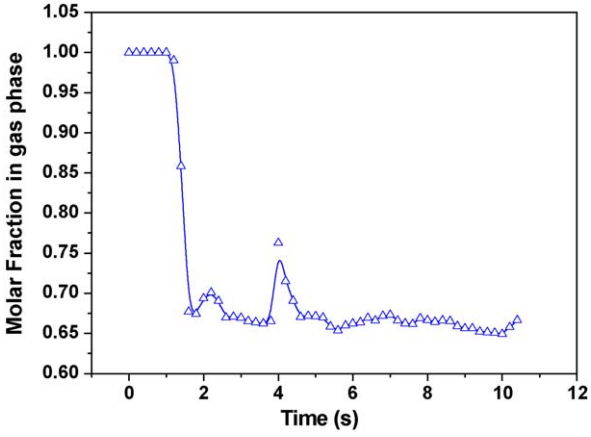


**Fig. 9.** The $H_2$ molar fraction at outlet.

## 5. Conclusions

A model has been presented that describes a multiphase hydrodynamics based on the kinetic theory of granular temperature applied to fuel reactor for chemical looping combustion process. Our recent thorough literature review shows that multiphase fluid dynamics modeling for CLC is not available in the open literature by FLUENT code.

The kinetic of the oxygen carrier reduction have been incorporated into the FLUENT code to model reactive fluid dynamic of fuel reactor. Computational results from the simulation show low fuel conversion rate partially due to fast, large bubbles rising through the reactor, low bed temperature and large particle size. To decrease the unburned hydrogen fuel in the flue gas, the nano-size oxygen carrier might be a preferred candidate because it does not generate large bubbles and hence increase the conversion of fuel gas in the reactor.

Similar to circulating fluidized bed combustor simulations where the riser was initially modeled prior to the complete loop, we modeled the critical component of the system, namely the fuel reactor. However, it is valuable to couple the fuel reactor with other components such as the air reactor and cyclone to model the complete loop system since the heat integration between chemical looping reactors is a very important feature in this novel technology development which can exploit the existing circulating fluidized bed technology.

## Acknowledgments

This work was financially supported by the National Natural Science Foundation of China (no. 50606006) and Hi-tech Research and Development Program of China (863 Program, 2006AA020101).

## References

Abad, A., Mattisson, T., Lyngfelt, A., Rydén, M., 2006. Chemical-looping combustion in a 300 W continuously operating reactor system using a manganese-based oxygen carrier. Fuel 85, 1174–1185.

Adánez, J., García-Labiano, F., de Diego, L.F., Plata, A., Celaya, J., Gayán, P., Abad, A., May 2003. Optimizing the fuel reactor for chemical looping combustion. In: Proceedings of FBC2003-063, 17th International Fluidized Bed Combustion Conference, Jacksonville, FL, pp. 18–21.

Adánez, J., de Diego, L.F., García-Labiano, F., Gayán, P., Abad, A., Palacios, J.M., 2004. Selection of oxygen carriers for chemical-looping combustion. Energy Fuels 18 (2), 371–377.

Byung-Su, Kim, Hong Yong, Sohn, 2002. A novel cyclic reaction system involving CaS and $CaSO_4$ for converting sulfur dioxide to elemental sulfur without generating secondary pollutants. 3: Kinetics of the hydrogen reduction of the calcium sulfate powder to calcium sulfide. Ind. Eng. Chem. Res. 41, 3092–3096.

Chejne, F., Hernandez, J.P., 2002. Modeling and simulation of coal gasification process in fluidized bed. Fuel 81, 1687–1702.

Cho, P., Mattisson, T., Lyngfelt, A., 2004. Comparison of iron-, nickel-, copper and manganese-based oxygen carriers for chemical-looping combustion. Fuel 83, 1215–1225.

Ding, J., Gidaspow, D., 1990. A bubbling fluidization model using kinetic theory of granular flow. AIChE J. 32 (1), 523–538.

Enwald, H., Almstedt, A.E., 1999. Fluid dynamics of a pressurized fluidized bed: comparison between numerical solutions from two-fluid models and experimental results. Chem. Eng. Sci. 54, 329–342.

Frazeli, A., Behnam, M., 2007. CFD modeling of methane autothermal reforming in a catalytic microreactor. Int. J. Chem. React. Eng. 5 (Article A93).

Gidaspow, D., Bezburuah, R., Ding, J., 1992. Hydrodynamics of circulating fluidized beds, kinetic theory approach. In: Fluidization VII, Proceedings of the 7th Engineering Foundation Conference on Fluidization. pp. 75–82.

Gunn, D.J., 1978. Transfer of heat or mass to particles in fixed and fluidized beds. Int. J. Heat Mass Transfer 21, 467–476.

Ishida, M., Yamamoto, M., Ohba, T., 2002. Experimental results of chemical looping combustion with $NiO/NiAl_2O_4$ particle circulation at 1200 °C. Energy Convers. Manage. 43, 1469–1478.

Johansson, M., Mattisson, T., Rydén, M., Lyngfelt, A., October 2006. Carbon capture via chemical-looping combustion and reforming. In: International Seminar on Carbon Sequestion and Climate Change, Rio de Janeiro, Brazil, pp. 24–27.

Johansson, E., Mattisson, T., Lyngfelt, A., Thunman, H., 2006b. A 300 W laboratory reactor system for chemical-looping combustion with particle circulation. Fuel 85, 1428–1438.

Mattisson, T., Jardnas, A., Lyngfelt, A., 2003. Reactivity of some metal oxides supported on alumina with alternating methane and oxygen—application for chemical-looping combustion. Energy Fuels 17, 643–651.

Mattisson, T., Johansson, M., Lyngfelt, A., 2004. Multicycle reduction and oxidation of different types of iron oxide particles—application to chemical looping combustion. Energy Fuels 18, 628–637.

Patil, D.J., Annaland, M.S., Kuipers, J.A.M., 2005. Critical comparison of hydrodynamic models for gas–solid fluidized beds—Part I: bubbling gas–solid fluidized beds operated with a jet. Chem. Eng. Sci. 60, 57–72.

Ravelli, S., Perdichizzi, A., Barigozzi, G., 2008. Description, applications and numerical modelling of bubbling fluidized bed combustion in waste-to-energy plants. Progr. Energy Combust. Sci. 34, 224–253.

Richter, H.J., Knoche, K.F., 1983. Reversibility of combustion process. In: ACS Symposium Series 235, Washington, DC, pp. 71–85.

Ryu, H.-J., Bae, D.-H., Han, K.-H., Lee, S.-Y., Jin, G.-T., Choi, J.H., 2001. Oxidation and reduction characteristics of oxygen carrier particles and reaction kinetics by unreacted core model. Kor. J. Chem. Eng. 18, 831–837.

Scott, C., Coronella, Charles J., 2005. CFD Simulation of particle mixing in a binary fluidized bed. Powder Technology 151, 27–36.

Spalding, D.B., Markatos, N.C., 1983. Computer Simulation of Multi-Phase Flows, CFDU, Imperial College, UK, pp. 36–50.

Tao, W.Q., 2000. Recent Advance of Numerical Heat Transfer. Science Press, Beijing.

Vasquez, S.A., Ivanov, V.A., 2000. A phase coupled method for solving multiphase problems on unstructured meshes. In: Proceedings of ASME FEDSM'00: ASME 2000 Fluids Engineering Division Summer Meeting, Boston.

Wen, C.Y., Yu, Y.H., 1966. Mechanics of fluidization. Chem. Eng. Prog. Symp. 62, 100–113.

Zafar, Q., Abad, A., Mattisson, T., Gevert, B., 2007. Reaction kinetics of freeze granulated $NiO/MgAl_2O_4$ oxygen carrier particles for chemical-looping combustion. Energy Fuels 21, 610–618.